Egyptian Journal of Chemistry

http://ejchem.journals.ekb.eg/

Synthesis and Application of Nanoporous Adsorbents Based on Natural Resource in Dye Removal from Water

Samar M.W. Ghonim [a,b*], Hanan F. Youssef [c], Mostafa Y. Nassar [a],Mohamed H. Shaltout [b], and Alaa S. Amin [a]

[a] *Chemistry Department, Faculty of Science, Benha University, Benha, Egypt*

[b] *Reference laboratory for drinking water, Holding Company for water and waste water, Cairo, Egypt*

[C] *Materials Technology and Mineral Resource Research Institute, National Research Centre, El-Buhouth Street, 12622, Dokki, Cairo, Egypt*

Abstract

The current work is devoted to investigate the zeolitization ability of locally available volcanic rock with alkali-Andesitic composition (AR), using the conventional hydrothermal technique under mild lab conditions of 1.0M NaOH, 140 ºC, and a duration of 1-3 days. The obtained product was a zeolite mixture (ZM) containing, Zeolite-W (synthetic analogue of Merlinoite zeolite (MER), Epistilbite (EPI), Zeolite-X (ZX), and Analcime (ANA). The efficiency of the formed ZM was tested as a novel inexpensive adsorbent for the removal of malachite green (MG) dye from contaminated water. The chemical composition and phases of the original rock and its alternative product mixture were investigated by XRF, XRD, SEM, EDAX techniques. To increase the removal efficiency, effecting parameters on adsorption process were investigated and optimized by batch design of experiments approach. Results indicated that, the adsorption isotherm was following Langmuir model with 91.66 mg/g a maximum adsorption capacity and the adsorption kinetics was most appropriately explained using pseudo-second-order model. Furthermore, the investigation of applying Dubinin Radushkevich has indicated that, the adsorption of MG is a physical process. Thermodynamics studies predicted an endothermic and spontaneous nature for the adsorption.

Keywords: alkali-Andesitic-rock; Hydrothermal route; Synthetic Zeolites; Zeolite-W; Epistilbite; Analcime; Zeolite-X; Dye removal.

1. Introduction

With the rapid rate of industrial development, the environment gets affected by many pollutants, produced within the manufacturing activities. A large quantity of water is used for various processing wherein effluents contaminated with organics, toxins and heavy metals are being continuously discharged into water resources and soils. This results in deficiency of oxygen because of growth of unnecessary organisms [1]. Synthetic dye is one of those effluents that has increased consumption amounts in the industrial procedures, because of its vast applications as in paint, cosmetics, textile, paper, printing, leather, plastics, electroplating, wool and pharmaceutics [2]. Dyes molecules in water can cause mutagenicity, carcinogenicity, and kidney dysfunction, liver, brain, reproductive system and central nervous system [3]. Malachite green dye (MG) is an organic cationic dye which is intensively used in the paper formulation, ceramics production, leather, textile industry, food coloring and cell staining. Its disinfecting action facilitates its normal use as anti-bacterial and anti-fungal agent in aquaculture industry against parasites, as well as, in the treatment of scratches on fish bodies[4]. Despite of all the benefits, MG and its reduced forms can be highly toxic, carcinogenic, and mutagenic due to the presence of the nitrogen in its structure [5]. This particular composition can cause serious effects on liver, kidney, intestine and gonads of aquatic organisms. Therefore, MG application was restricted in many countries in aquaculture industry. In the

*Corresponding author e-mail: samrwheep0712@gmail.com.; (Samar M.W. Ghonim).
Receive Date: 02 January 2022, Revise Date: 17 January 2022, **Accept Date:** 18 January 2022
DOI: 10.21608/EJCHEM.2022.114237.5195

same context, the complex chemical structures of dyes resulted in environmental resistance to degradation thus, cost-effective and highly efficient technology of adsorption has widely been applied to treat dye-containing wastewater[6].

Zeolites (Z) are hydrated porous, aluminosilicate, inorganic solids with high crystallinity, made up of tetrahedral $[SiO_4]^4$ and $[AlO_4]^5$ units, linked via oxygen atoms in an infinite 3D framework [7]. Those valuable materials are used as adsorbents, ion exchangers and catalysts [8]. Additionally, Zeolites have an economic aspect since they are inexpensive with large natural abundance, with non-toxic effects, and possessing high surface area [3]. Zeolites are found naturally in the mineral resources or can be prepared synthetically from Si and Al precursors. Natural zeolites (Examples; Clinoptilolite, Faujasite, Analcime, phillipsite, Heulandite, etc..) were found to show good efficacy in adsorbing malachite Green (MG) in aqueous solutions [9]. Although having the ability for water treatment, natural zeolites have many disadvantages containing; mixed type presence with heterogenous porosity, impure nature, not mined in many countries, and expensive if imported. Thus, production of zeolites from available local Si&Al-sources can help effectively in finding a synthetic alternative with feasible cost. Synthetic zeolites were used successfully in treating wastewater containing dyes; 3A zeolite (synthetic Z) was able to eliminate a significant amount of Rhodamine B and MG from environmental water samples,[10]; zeolites prepared from two types of metakaolin were positively used for adsorbing methylene blue, safranin, and MG from aqueous solutions [11].

Due to multiple industrial and environmental needs, several methods for obtaining Z from different sources of silicon and aluminum were exploited [12]. Sustainable routes are withdrawing all the attention for being environmentally of non-harmful paths and using cost effectiveness in its formation. Hydrothermal processing is a very attractive method that usually applied for the precursor (raw sources, solid wastes, etc.) conversion into Z valuable products [13]. Table 1 shows some of the published data for the same zeolite-types obtained in the current work, their starting materials, preparation conditions and applications are also given.

Andesite is a grey volcanic rock named in reference to the Andes Mountain where it is dominated. Naturally, it exhibits fine-grained (very fine particles) or porphyritic (contains large crystals in very fine matrix) texture with a chemical composition of 50-60% silica, about 5% of K_2O+ Na_2O alkalis, CaO contents of 6-7 %, along with some MgO and Fe-oxides [35]. Mineralogically, it contains andesine and oligoclase as plagioclase feldspars, one or more of the dark ferromagnesian minerals such as pyroxene and biotite. Sometimes, many gas bubbles were left after the solidification of lava (volcanic magma), those voids are often filled with later mineralization, usually zeolites [35].

Generally, Andesite rock was commonly used in architecture, construction of roads and sculptures, making tiles, landscaping and monuments formation due to its known heat and frost resistant ability [36]. Meanwhile, porphyritic-type andesite, named as “wheat rice stone” (WRS) has shown adsorption ability and bioactivity due to vesical porosity and cation dissociation. Therefore, WRS was extensively used in treating water and ammonium-rich swine waste [37]. Regardless of its porous nature, andesite maintains limited, differently-sized and non-uniformly distributed voids, which hindered its specific industrial use. Hence, the rock conversion into zeolites with definite and even porous structure in the nano-scale-size can certainly widen its application at very low cost, especially in the field of wastewater treatments such as dyes and heavy element removal [38]. Zeolites prepared from natural and/or chemical ingredient have been utilized in water purification, some of which are given in the previous Table 1.

Merlinoite (MER) is a rarely-found natural zeolite mineral that was originated in different geological conditions, especially in the massive volcanics and intrusive marine sediments. Its typical chemical formula is given as; $(K, Na)_5(Ca, Ba)_2Al_9Si_{23}O_{64} \cdot 23H_2O$, or $K_6\ Ca_2\ Na\ [Al_{11}\ Si_{21}\ O_{64}].22H_2O$ [39]. Zeolite W is the synthetic analogue of the natural Merlinoite which has been prepared from various precursor gels of different chemicals and natural rocks such as rhyolitic pumice [40]. It possesses small-pores and its channel system is constructed from 3D interconnected 8-membered ring (8 MR) pores and has intermediate composition of $2<Si/Al<5$[41]. Synthetic zeolite W has been applied as a membrane for gas separation, catalyst support, fertilizer in agriculture field, and ion-exchange material [15-16, 42].

Zeolite type	Starting material	conditions	Application	Ref.
Zeolite W (MER) $(K, Na)_5(Ca, Ba)_2Al_9Si_{23}O_{64}\cdot 23H_2$	KOH, soluble silicate, Na AlO_2, NH_4Cl	170 °C /22 h	K-extraction	14
	Amorphous silica+ Al $(NO_3)3.9H_2O$	250 °C/ 8h	Cs^+& Sr^{2+} removal	15
	Coal fly ashes, KOH	150-200°C/8-24 h	slow-release K-fertilizer	16
	Water glass, Na AlO_2, KOH	170°C/ 22h	K^+ ion extraction	17
	Ludox, Al $(OH)_2$, KOH	165°C/72h	No application	18
	Silica acid, Al $(OH)_3$, KOH	165°C/ 72h	No application	19
	TEOS, Aluminum tri-sec-butoxide,KOH, [organometallic Si &Al and precursors.	165°C /48 h	No application	20
	Silica sol, $NaAlO_2$, KOH	165°C/ 72h	No application	21
Analcime (ANA) $Na_{16}[(AlO_2)_{16}(SiO_2)_{32}]$ $.16H_2O$	Kaolin+ Ludox+ NaOH	150 ^{O}C/4h	Hydrogen storage	22
	NaOH, Silica fume, HCl, Al $Cl_3.6H_2O$, glutamic acid& L-arginine	120 °C /24h	Removal of Pb^{2+} &Cu^{2+}	23
	Abandoned soil, NaOH+ SiO_2	180 °C /12 h.	Cu-capturing from soil	24
	sorghum ash Si, Na-aluminate, NaOH	120 °C/24 h	Electrooxidation of Formaldehyde	25
	Kaolin+ Na-silicate soln.+NaOH	200 °C for 24 h	$Pb^{2+,}$ Cu^{2+}& Ni^{2+} Removal	26
	Rice husk ash and kaolin	180 °C /24h, 72 h.	adsorption of phenol	27
	Natural Analcime + argillite	Grinding to 0.25–0.5 mm.	Adsorption of U, Ra &Th	28
Epistilbite (EPI) $(Ca, Na_2)_3(Al_6Si_{18}O_{48}).$ $16H_2O$	Natural epistilbite	Natural	Adsorbing greenhouse gases, CO_2 and NO_2.	29
Zeolite-NaX $(Ca,Mg,Na_2)_{29}(H_2O)_{240}$ $Ca_{23.2}Mg_{22.4}(Al_{92}Si_{100}O_{384})$	Rice husk ash + NaOH + $NaAlO_2$	90 °C /24 h	Removal of CO_2 From Industrial Exhaust gas stream.	30
	Diatomite + NaOH + Al $(OH)_3$	110°C/ 3-5h	-	31
	Diatomite + NaOH+ $NaAlO_2$ + thiourea	90°C /20h	removal of Cd^{2+}	32
	Coal fly ash + NaOH	90°C/ 6h.	As (V) removal from Wastewater	33
	$Na_2SiO_4\cdot 9H_2O$, $NaAlO_2$, four ethyl ammonium hydroxide, silane, glutaraldehyde solution + $(NH_2OH\cdot HCl)$	100°C / 16 h.	Adsorption of Ru^{3+} from wastewater	34

Epistilbite (EPI), is also a small pore-size zeolite, it has a two-dimensional 8 × 8 pore architecture [43]. This zeolite possesses a system of channels with pore openings dimensions of 0.37 nm ×0.45 nm and 0.36 nm × 0.36 nm in [001]and [101] directions, respectively. Maximum diameter of a sphere that can be included in the EPI voids is 0.547 nm; diameters of the spheres that can diffuse along the channels in the [100] and [101] directions are 0.362 nm and 0.348 nm, correspondingly. The chemical composition of this alkaline-earth zeolite is (Ca, $Na_2)_3(Al_6Si_{18}O_{48}).16H_2O$ with a Si/Al ratio close to 3 [44]. Dominant cation for EPI zeolite is always Ca^{2+}, it comprises 65% to 90% of the non-framework cations; Ba^{2+} and K+ are minor components in all the analyses [44]. Epistilbite is poorly studied zeolite with few numbers of registered patents which proposed its possible uses. It may serve as de-NOx catalyst that provides superior NO control performance without substantial changing or affecting the hydrocarbon conversion during the FCC process [45] or functionalized silicate nanoparticles to remove the asphaltene particles[46]. This zeolite, among others, is recommended as activating additive in the cleaning liquid [47].

Analcime (ANA) zeolite is the smallest-pore zeolite with Si/Al ratio of 1.8-2.8, pore opening of 0.26 nm in diameter, and a channel dimension of 0.42 x 0.16 nm. ANA shows a compact and dense structure compared to all zeolites, the idealized unit cell has $Na_{16}Al_{16}Si_{32}O_{96}\cdot 16H_2O$ composition [48]; its complex structure, indicates corner sharing [SiO_4] and [AlO_4] tetrahedron, in manner of irregular channels and some cavities occupied by the exchangeable Na-ions in the crystal lattice [40]. Analcime is usually of cubic symmetry, but can also be of orthorhombic and tetragonal ones. The unit cell contains 4-,6-, and 8-membered oxygen rings that build three, non-intersecting channels [49]. Every Na^+ is surrounded by 4 oxygen ions and 2 water molecules, which results in a distorted octahedron [50]. Analcime displays a variety of applications in technology, especially in selective adsorption in wastewater treatments [23-24] and heterogeneous catalysis [51]. Analcime is also successfully used as fertilizer dispenser in agriculture [52], in the nano electronic field [53], in stomatology, i.e. in ceramics for denture [54].

Zeolite X (ZX) is a member in the aluminosilicate molecular sieves (industrial zeolites) with Faujasite-type structure (FAU), high-Si/Al-ratio, and a typical formula of (Ca, Mg, $Na_2)_{29}$ $(H_2O)_{240}|$ $[Al_{58}Si_{134}O_{384}]$. FAU Framework implies 24 tetrahedra (cuboctahedra) units (sodalite cages), arranged in the unit cell in a manner likes that of the carbon atoms in diamond assembly. They are connected via hexagonal prisms (double six rings) in a 3D porous channel structure. It maintains 12 oxygen ring window openings with 8 Å aperture and 12 Å super cages [55].The structure exhibits large surface area, wide channels, and cages with large openings which results in large adsorption capacity with good cationic exchange properties [56]. ZX has been utilized in drug delivery, wound healing and studies on endocytosis [57], as well as, in CO_2 selective adsorbency from gas streams, and pre-purification of air for industrial air separation [30]. Due to the excellent cavities and pore openings, ZX has obtained much attention in the fields of catalysts[58], ion exchanger, molecular sieves, adsorbents[59].

The current study aims at investigating the feasibility of converting an inexpensive and locally available natural resource (Andesitic rock) in the synthesis of zeolites using an easy and simple method (Conventional hydrothermal treatment), using the alkali effect of caustic soda at relatively low temperature of 140 °C for 1-3days. The efficiency of the synthetic product will be tested in the removal of Malachite green dye from waste water. The chemical and mineralogical composition of the original rock and that of the synthetic zeolite mixture are to be examined, parameters affecting the adsorption process will be optimized and the thermodynamic parameters are to be discussed, as well.

2. Materials and Methods

2.1. Chemicals and materials

(A) For zeolite preparation, the starting material, Andesite rock, was supplied by Egyptian mineral resources authority, as a massive hand specimen. Sodium hydroxide pellets (98.6% NaOH) and Malachite green (MG) dye $C_{23}H_{25}ClN_2$, molecular weight: 364.91 from (Sigma-Aldrich) 99% (dye content). Potassium Mono-basic KH_2PO_4, Molar mass 136.09 g/mol, (98.0-100.5%), Potassium di-basic K_2HPO_4 Molar mass 174.18 g/mol, (98.0-100.5%) and Calcium Chloride molecular Formula $CaCl_2.2H_2O$, Molar mass 147.02 g/mol (99.0-103.0%) were purchased from Panreac.

2.2. Zeolite Synthesis

Figure 1 shows the flow chart for the hydrothermal processing used for the synthesis of

zeolite phases from Andesitic rock. In a typical lab work, the rock powder of particle size <40 µm was treated with 1.0 M NaOH solution, the use of the least alkali concentration is to benefit from the natural alkali and alkaline-earth cations contents maintained in the original rock composition. The batch constituents were stirred for 7 days at 700 rpm and room temperature to dissolve the rock powder and formation of Si and Al precursor slurry or fresh gel. About 50 ml of the prepared slurry was placed in a locally manufactured, 125 ml Teflon-lined stainless-steel vessel, and heated at temperature 140 ºC for 1-3 days. The treated samples were then collected, washed severally with distilled water using centrifugation at 4000 rpm for solid/liquid separation. Solid product was then collected and dried overnight at 140 ºC for phase characterization testing.

Figure (1): Schematic presentation of the andesite rock-batch Zeolite conversion via hydrothermal method.

2.3. Adsorption testing (Adsorption batch experiments)

The batch experiments were carried out according to Mittal et al. [60] to study the efficiency of the prepared material in eliminating the MG dye from aqueous solution. The optimal conditions for the removal processes, such as solution pH, zeolite dose, initial concentration of M.G, contact time, ionic strength and temperature were investigated. Batch experiments were achieved at room temperature by the addition of known weight of zeolite product into a number of 100 ml glass conical flasks, sealed with aluminum foil on a rotary shaker at 250 rpm, containing 50 mL of MG solution in deionized water. The effect of pH was conducted to by shaking 0.2g of zeolite product at different pH values from 3 to 10 with 50 ml of MG solution 10 µg/l for 15 min. pH values was adjusted by phosphate buffer solution and 0.1 M HCl or 0.1 M NaOH. The effect of adsorbent dosage was conducted by adding desired amounts of zeolite product 0.01, 0.025, 0.05, 0.1, 0.2, 0.3, 0.4 and 0.5 g at the optimal pH pH 7 with 50 mL of the M.G solutions (10µg/l) in distilled water. To investigate the effect of M.G concentration, experiments were processed by adding 0.2g of zeolite product at optimal pH pH 7 to 50ml of MG solutions, having different MG concentrations of 2, 5, 10, 15, 20, 30, 40, 50, 70, 90,100,120,150,300,400,600,800 and 2000 mg/l. Equilibrium time was conducted by shaking 0.2g of zeolite at optimum pH and MG solutions of 800 mg/l in distilled water for different time intervals of 5, 10, 60, 90, 120, 150, 180,210,240,300 and 320 min. To investigate the effect of temperature, thermodynamic experiment was conducted at optimal pH 7.0 for, optimal concentration 800 mg/l for, optimal adsorbent dose 0.2g at equilibrium time of 120 min for different temperatures of 35, 45 and 52 °C. To examine the effect of ionic strength, experiments were done at different concentrations of $CaCl_2$ of 0.01, 0.05, 0.1, 0.3, and 0.5 M, at optimum conditions that mentioned previously. It is noteworthy that the percent removal of malachite green dye (% Removal) at different PH , zeolite dosage (g), different concentrations of malachite green dye (2-2000 mg/l), time (5-320 min) and different concentrations of $NaCl_2$ (0.01- 0.5 M) was estimated using Eq. (1)

$$\%\text{Removal } (R\ \%) = (C_o - C_e)\ 100/C_o \quad \textbf{(1)}$$

Where, Co (mg/l) is the initial concentration of malachite green dye solution, C_e is the residual concentration of malachite green dye Moreover, the effect of different concentrations of malachite green dye (2-2000 mg/l) has been studied as the adsorption capacity of the adsorbent at equilibrium (Qe, mg/g) was measured using Eq. (2).

$$Q_e = (C_o - C_e)\ v/m \quad \textbf{(2)}$$

Where, C_e (mg/l) is the concentration of malachite green dye solution at equilibrium.

2.4. Characterization techniques

The chemical composition of the rock precursor was studied using Wavelength Dispersive X-Ray Fluorescence Spectroscopy; Axios advanced, sequential WD XRF spectrometer, PANalytical 2005. The identification of rock and product phases were done via X-ray diffraction instrument, BRUKUR D8 ADVANE with secondary monochromatic beam CuK radiation at keV = 40 and mA = 40 was applied. The diffraction charts and relative intensities are

obtained and compared with ICDD files. Whereas, the surface morphologies and the internal microstructures were studied using SEM (Quanta 250 FEG, Field Emission Gun) attached with EDX Unit, with accelerating voltage 30 kV (FEI, Netherlands).

For the adsorption batch experiments, pH meter model (Hach, Sension1) equipped with reference electrode was used to adjust the solutions pH. The following equipmentes were also used; rotor shaker with 15 position model (THERMO, SHKE2000) supported with timer, Analytical balance with four digits (Sartorius), Oven (Binder), Centrifuge model (Hermle, Z206A) for solid/liquid separation at 6000 rpm, water bath (Memmert) for solution temperature adjustment, and a Spectrophotometer model (analytik jena, specord 205 wavelength range (190:1100 nm).

3. Results and Discussion

3.1. Rock characterization

The XRF testing of the andesitic rock revealed the following oxide ingredients as the main constituents (in weight %); 44.80 SiO_2, 16.30 Al_2O_3, 13.70 Fe_2O_3, 11.20 CaO, 6.89 MgO, 1.59 Na_2O, 1.16 K_2O, 1.27 TiO_2, 0.16 P_2O_5, 0.08 SO_3, 0.18 MnO, and some minors comprising; NiO, SrO, Cr_2O_3, Co_3O_4, CuO, ZnO &Cl of 0.31%, whereas, the L.O.I was 2.36% of the total rock weight. Notably, the high percentage of alkali-cations (Ca, Na, K, Mg, etc.) reflected the alkali-rich nature of the andesitic rock. It is worth mentioning that, the utilization of such precursor is costly- effective in respect to zeolite production owing to the fact that, the hydrothermal preparation of zeolites usually involves a step of alkali- rock treatment.

Table 2 and Figures 2 are presenting the mineralogical composition and internal microstructure for the parent andesitic precursor, as given by XRD and SEM testing, respectively. As can be noticed from Figure 2A, the XRD diffraction pattern reflects a poor-crystallinity of the starting material where all phases were of reduced peak intensities. In the same time, Figure 2B presents the SEM micrographs of the rock internal texture where, very few large fragmented crystals (phenocrysts) are scattered within a fine-grained glassy groundmass, mostly of the same chemical composition of those crystals. In general, the amorphous mode of the volcanic rocks typically specifies a sudden or rapid cooling of the molten volcanic magma (Lava). This usually indicates poor developing textures with minor amounts of fine crystalline phases (H, A, C & Q in this case) resulted in unfavorable crystallization conditions of insufficient gradient cooling an/or duration. The SEM result agrees well with the XRD finding of having incomplete and low intensity set of peaks for all detected phases, Figure 2A.

Table 2: Mineral composition of Andesite rock.

Ref. Card	Mineral Name	Chemical Composition
00-04	Magnesiohornblende, ferroan	Ca2 (Mg, Fe+2)4 Al (Si7Al) O22 (OH, F)2
00-04	Anorthite, Sodian, disordered	(Ca, Na) (Si, Al)4 O8
00-04	Clinochlore	(Mg5Al (Si, Al)4O10 (OH)8
00-00	Quartz, low-alpha	SiO2

A). XRD **(B). SEM**

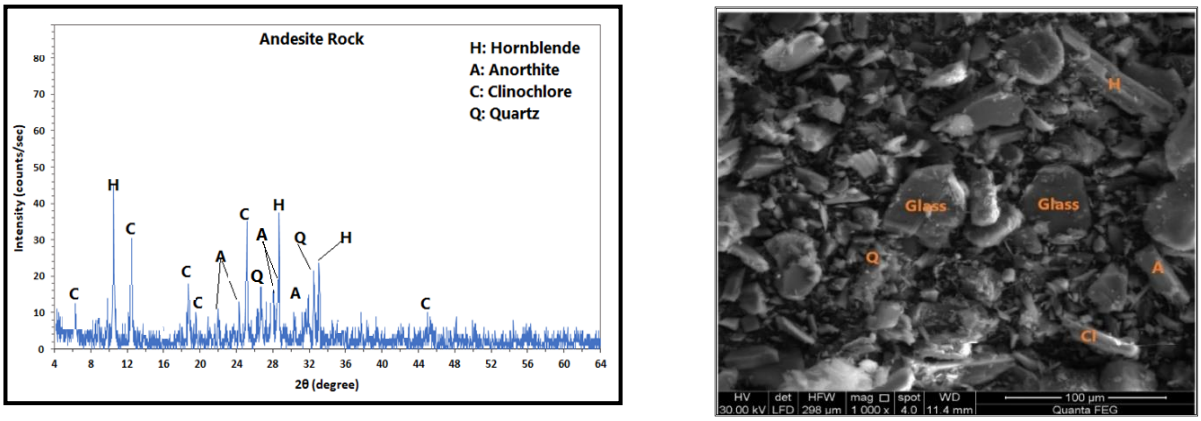

Figure 2: XRD profile (A) and SEM (B) microstructure for the starting andesitic rock, where; H is Magnesiohornblende, A refers to Anorthite, C is clinochlore, and Q is the quartz.

3.2. Characterization of Zeolite product

3.2.1. XRD Results

Table 3 and Figure 3 are displaying the obtained zeolite phases developed after attacking the rock powder with 1.0 M NaOH for 7days, followed by hydrothermal treatment at 140 °C for 1(a), 2 (b), and 3 (c) days. The synthetic powder was then tested using the XRD tool and the formed phases were compared with the standard PDF cards. The recognized batch materials were of the following compositions and identities of Table 2. It is clear that, the Zeolite-W (W), Epistilbite (E), and Zeolite-X were the main developed phases in the batch product from the first day of treatment, Analcime (A) was then appeared in the obtained powder after two days of the reaction and afterwards.

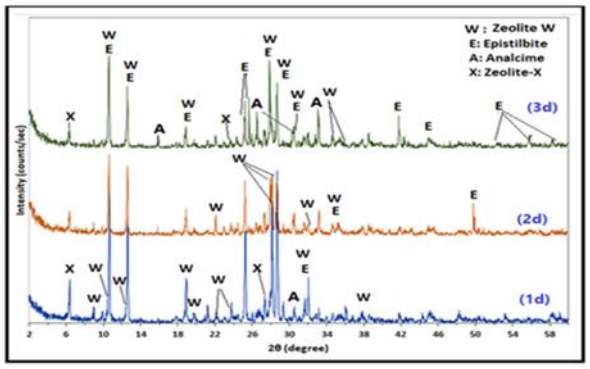

Figure 3: XRD profile for the final phases developed in the the synthetic batch- product at 140 °C/ 1-3days.

The main phase Z-W contained Potassium as its main cation, along with less amounts of sodium and calcium, the Si/Al (2.45) is consistent with that of the literature [41]. In the other hand, EPI contained calcium as the only modifying cation and the Si/Al was 2.88 which also agrees with the theoretical ration which is close to 3[44]. The Si/Al for analcime appeared in its matched formula in the XRD data base was found to be 2, which is exactly within the reported range of 1.8-2.8. Zeolite-X with Si/Al ratio of 1.1 which is lower than the theoretical value of 2-3, this Si deficiency in ZX composition could be related to the low-silica contents of the parent andesitic rock, 44.80 wt%.

3.2.2 SEM and EDS

Figure 4 presents the internal microstructure of the developed phases and their microchemical analysis. Figure 4A is showing prismatic shaped crystals of Zeolite-W(W) with a well-developed and differently-sizes particles in the range of 3-5 μm in length; Epistilbite (E) appeared in a lath-shaped particles with more elongated form of about 5-10 μm in length and up to 1 μm in width (Figure 4B); Analcime (A) implied spherical granules with 1-2 μm (Figure 4C); and finally, Zeolite-x exhibited a bipyramidal cubic morphology with well-formed crystals of 2-5 μm (Figure 4D). The obtained data ascertained the XRD result of having W, E, and ZX as the dominant phases, accompanied by smaller amounts of analcime in the final stage of crystallization.

Table 3: Mineral composition of the synthetic product. synthetic batch- product at 140 °C/ 1-3days.

Ref. Card	Mineral Name	Chemical Composition	Si/Al
[61]	Zeolite-W (MER)	$Na_{0.68}K_{5.28}Ca_{1.844}Mg_{0.444}(H_2O)_{19.44}$ $[Si_{22.72}Al_{9.28}O_{64}]$	2.45
01-019-0213	Epistilbite (EPI)	$Ca_{3.06}(Al_{6.18}Si_{17.82})O_{48}.16\,H_2O$	2.88
00-003-0740	Analcime (ANA)	$Na\,Al(Si\,O_3)_2 \cdot H_2O$	2
01-079-1131	(Ca, Mg)-Zeolite-X	$(Ca_{23.2}Mg_{22.4}(Al_{92}Si_{100}O_{384})$	1.1

Figure 4 is also showing the chemical microanalysis of the developed phase in the final product. Each table reding is presenting an average of three detected spots on differently-sized crystal-surfaces of the same zeolite phase (particles with different generations). Table 3 is tabulating those EDS elemental analysis of the scanned phases. The calculated Si/Al ratios were 2.3,1.98, 2.4, and 1.59 for Zeolite-W, Epistilbite, Z-x, and Analcime, respectively. Obviously, the deficiency in the silica content of the rock precursor is preserved in the composition of the synthetic product, especially that of zeolite-X. In addition, the prepared zeolites indicated total alkali contents of a higher amounts than that found in their theoretical formulae, as given from the XRD reference cards and EDS analysis. This finding agrees will with the alkali enrichment of the precursor rock composition, as mentioned in section 3.1. In addition, this can be explained in the light of the cation exchange property, known for all zeolites, where the early developed phases can replace their cations by other ones, released from the late dissolution of the rocky materials.

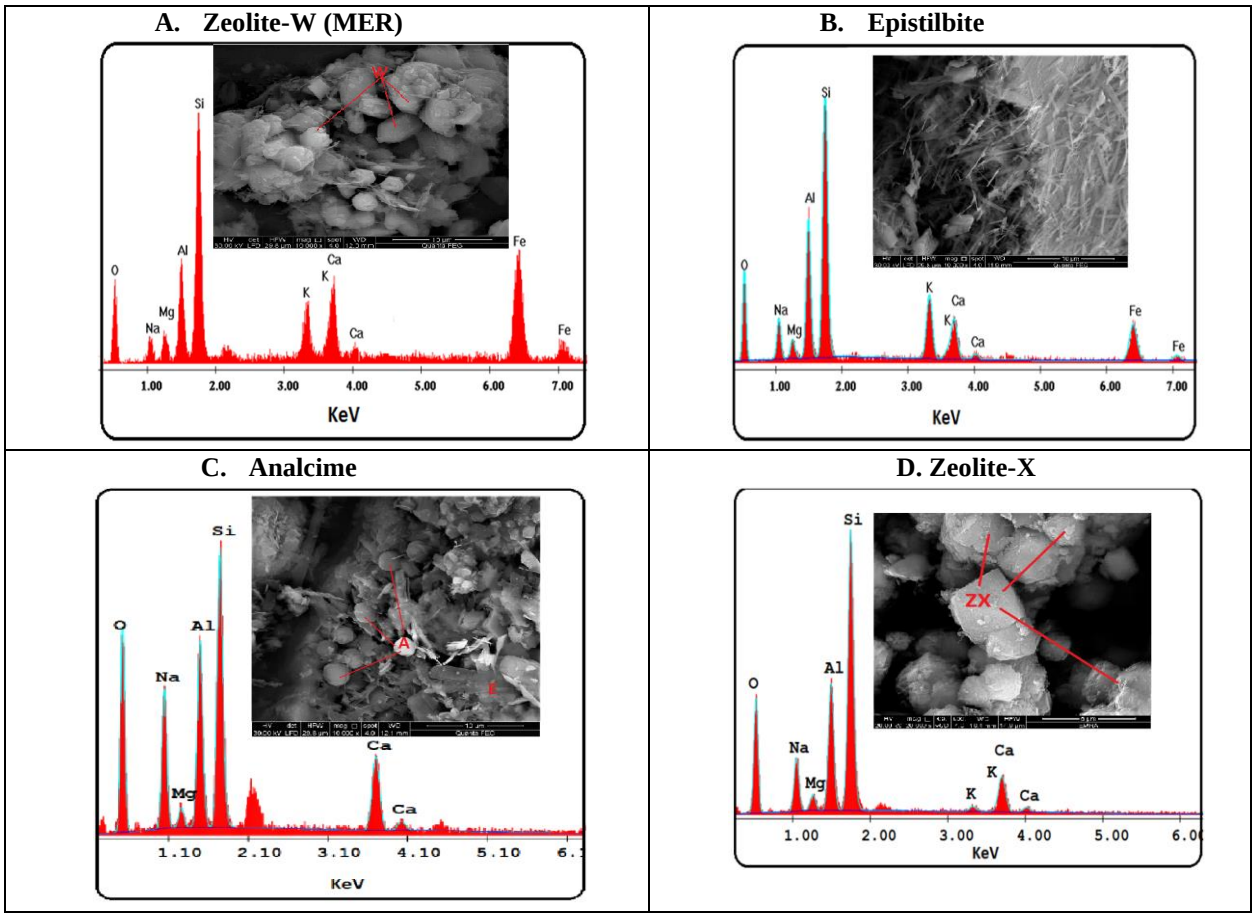

Figure 4: SEM micrographs for the synthetic product where: W: Zeolite-W, ZX: Faujasite-X, A: Analcime, & E: Epistilbite.

Table 4: EDS microanalysis for the synthetic product

Elements	Zeolite-W (MER)		Epistilbite (EPI)		Analcime (ANA)		Faujasite-X (ZX)	
	Wt%	At %	Wt%	At %	Wt%	At %	Wt%	At %
O K	24.16	40.10	29.70	44.23	40.17	53.06	35.84	49.47
Na K	4.78	5.52	7.13	7.38	15.18	13.95	9.11	8.75
Mg K	3.77	4.12	2.60	2.55	2.03	1.77	2.27	2.07
Al K	9.63	9.48	13.60	12.01	13.92	10.91	13.03	10.66
Si K	23.10	21.84	28.04	23.79	22.89	17.30	32.20	25.32
K K	4.95	3.36	6.69	4.07	--	-	0.60	0.34
Ca K	6.73	4.46	4.43	2.63	5.71	3.01	4.15	2.29
Ti K	3.01	1.67	---	--	-	-	-	-
Fe K	19.87	9.45	7.82	3.34	-	-	2.80	1.11
Total	**100**	**100**	**100**	**100**	**100**	**100**	**100**	**100**

Due to multiple mineralogical and chemical composition of the natural volcanics, their hydrothermal treatment is commonly resulted in an impure zeolitic product due to the complexity involved in the phase-dissolution process. In such case, the reaction system is actually a heterogenous one, containing differently-reacted materials with many controlling factors of disintegration, such as chemical composition, pH, crystallinity, rate of phase dissolution, and phase percentage, etc. [62]. It has been found that, zeolite formation was significantly affected by the concentration and type of the alkalis offered to the reaction solution by the susceptible dissolution of the rock ingredients [63]. The high alkalinity plays an enhanced rule in the materials dissociation process and mostly controls the proper

supply of the essential elements (Si, Al, and Cations) needed for zeolite framework construction. Herein, the mechanism of zeolite synthesis involves the spontaneous arrangement of SiO4 and AlO4 tetrahedral species around the hydrated cations, which act as a positively-charged directing agent in the formed gel, to facilitate and stabilize the phase crystallization [63a-c]. In addition, high alkalinity was proved to increase the precursor solubility and to provided more (OH^-) mineralizing agent for improving the rate of nucleation and crystallization of the microporous species [63a, 63c, 63d, 64].

3.3. Results of the dye adsorption

3.3.1. Effect of pH

The point of zero charge (pH_{ZPC}) of the applied zeolite mixture (ZM) used for the adsorption experiment is determined by using adsorbent to liquid ratio of 1.0:1000. For this, 0.1mg of ZM is added to 100 mL of water with varying pH values from 2.0 to 11 and stirred for 24 h. The pH values were adjusted by phosphate buffer solution and 0.1 M HCl or 0.1 M NaOH. The obtained ΔpH ($pH_{final} - pH_{initial}$) of the solution is plotted against the initial pH values, Fig.5.

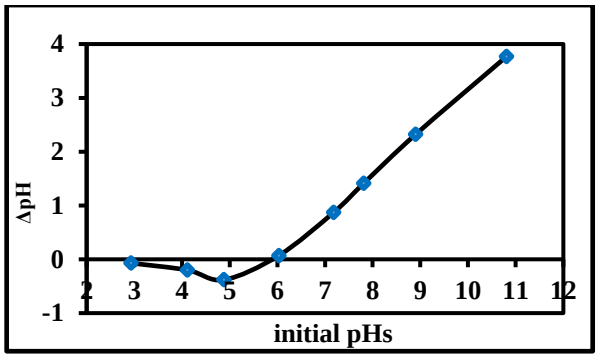

Figure 5: Zero-point-of-charge for zeolite product

As seen from the previous figure, the detected point of zero charge (pH_{ZPC}) for zeolite adsorbent was at pH 6.0 [65].

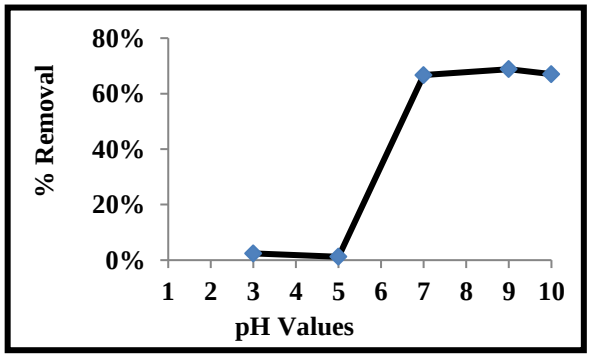

Figure 6: Effect of pH on the removal % of MG

The initial pH of the dye-contained solution is one of the essential parameters that influence the adsorption capability. The pH of a solution will affect: (1) the adsorbent surface charges, (2) the ionization degree of adsorbate molecules, and (3) the degree of dissociation of the functional groups found on the adsorbent active spots. **Fig.6** shows the adsorption of MG over zeolite product at various pH values, based on initial dye concentration of 10 mg/l MG, zeolite dosage 0.1 g and contact time of 15 min. It is obvious that, there is an improvement in the MG uptake over ZM surfaces when elevating the pH from 5.0 to 7.0. In contrast, any more increase in pH values over than 7.0 up to 10.0 indicated insignificant rise in the dye sorption. The structure of the dye molecule and the point of zero charge (pH_{ZPC}) of the ZM may explain the difference in dye uptake with respect to the initial solution pH. At a lower pH, the carboxylic groups of MG (pKa = 10.3) were protonated and had a high positive charge density [66], while ZM's point of zero charge is calculated to be 6.0, [67]. At a pH higher than pH_{ZPC}, the zeolite product particle acquires a negative surface charge and favors uptake of cationic dyes due to the increase of the electrostatic force of attraction. On the other hand, at low pH values, due to formation of positive charge on the surface of zeolite and protonation of dyes little electrostatic interaction occurs[10]. Due to this explanation, there is an electrostatic repulsion between dye molecules and zeolite product that causes the reduction in dye adsorption. The previous outcome was confirmed by Rahmani et al.[10]who showed the direct relation between the dye solution pH and the significant MG dye- removal of the synthetic zeolite 3A which was maximized at pH= 7.0, any further increase in the solution pH in the range of 7.0 to 9.0 was found insignificant in terms of dye sorption. In the same context, brilliant green adsorption efficiency on zeolite-Y, incorporated karaya gum hydrogel composite, was improved by raising pH and reached to the equilibrium value of 78% at pH 6, no noticeable change has been detected on further solution pH elevation [60].

3.3.2. Effect of adsorbent dose

Fig. 7 is showing the adsorption profile of MG versus different adsorbent amount in the range of 0.01–0.5 g/50 ml with initial concentration of 10.0 mg/1, and 15min contact time.

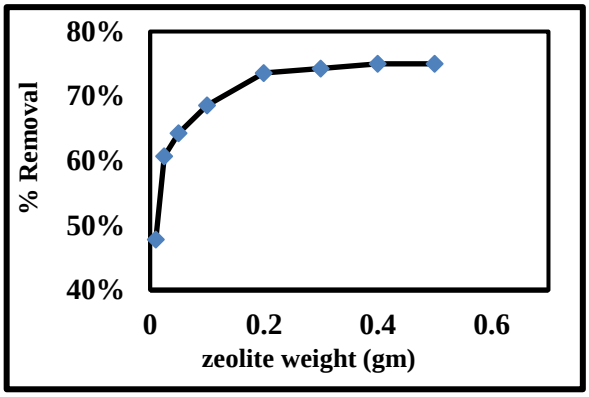

Figure 7: Effect of zeolite weight on the removal Of MG%

It is clear that, the percentage of MG removal has a direct relation to the adsorbent dose. Such a trend, is mostly attributed to an enlargement in the adsorbent surface area and the availability of more active adsorption sites. Although the percentage removal of dye is directly proportional to the adsorbent dose, the equilibrium adsorption capacity for MG is declined with the addition of more amounts of the synthetic product. Experimentally, the maximum dye removal of 73.5% was recorded at 0.2g/50 ml, after which no significant change in the adsorption yield occurred whatever the increase in adsorbent dose. This can be explained as follows, the addition of more zeolite powders resulted in different particles agglomeration leading to the adsorption sites blocking and in turn, the reduction in the available surface area ended with non-improved sorption performance [60]. This result has been confirmed by Rahmani et al.,[10] who reported the same finding when increasing 3A zeolite dosage in the removal of malachite green and Rhodamine B [10]. As well, Mittal et al. [60], on his work on eliminating brilliant green with 0.02 g/50 ml of zeolite-Y incorporated hydrogel composite of gum karaya (ZHC-4) with a max. efficacy of 98%.

3.3.3. Effect of Initial dye Concentration

Fig. 8 is showing the adsorption profile of MG versus different MG concentrations (50ml) in the range of 2.0–2000 mg/l with optimum PH 7.0 and optimum ZM dose of 0.2g and contact time of 15min.

The effect of different initial dye concentrations on the adsorption onto zeolite product is presented in **Fig. 8**. It could be noticed that, the removal percentage of MG has been decreased by increasing the initial dye concentration. This can be explained by the mass transfer driving force being provided by the initial concentration of the dye. The number of activated sites on the adsorbent is too high at lower concentrations, and any addition of dye molecules could interfere with them. Furthermore, because of the saturation of active sites on zeolite surfaces at higher dye concentrations, a lower removal percentage was observed [10]. This effect led to an increment in equilibrium sorption until the sorbent saturation was achieved with maximum adsorption capacity (q_{max}) 91.66 mg/g. Similar results were reported for adsorption of malachite green from environmental water samples onto 3A zeolite. The results showed that, the removal percentage of M.G decreased by rising the initial dye concentration from 10 up to 15mg/l for MG and from 15 up to 20mg/l for Rhodamine B[10].

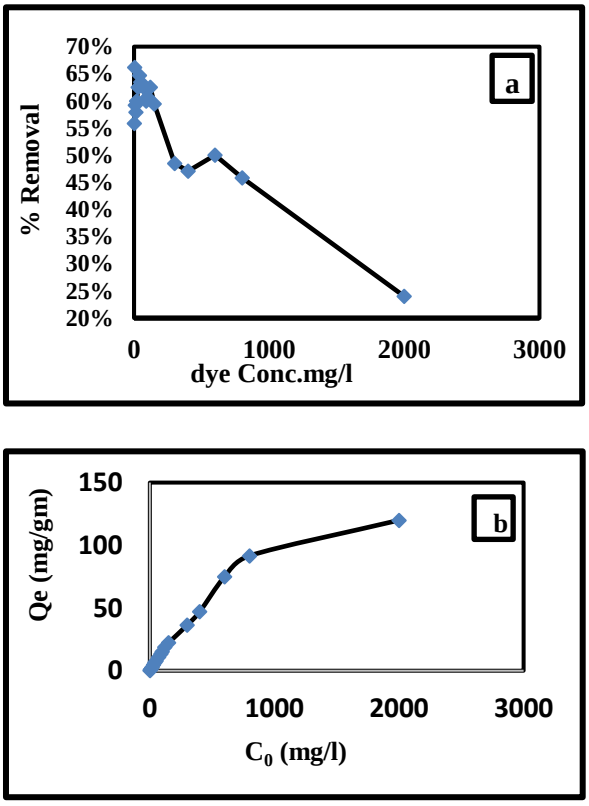

Figure 8: (a) Effect of initial concentration on removal % of MG at ZM dosage 0.2g/50ml, (b) Effect of adsorption capacity of ZM against initial concentration of MG at ZM dosage 0.2g/50ml.

3.3.4. Effect of Contact Time

Fig. 9 is showing the adsorption profile of MG versus different time intervals in the range of 5 - 320 min, with optimum pH 7.0, optimum ZM dose of 0.2g/50 ml and optimum dye concentration of 800 mg/l.

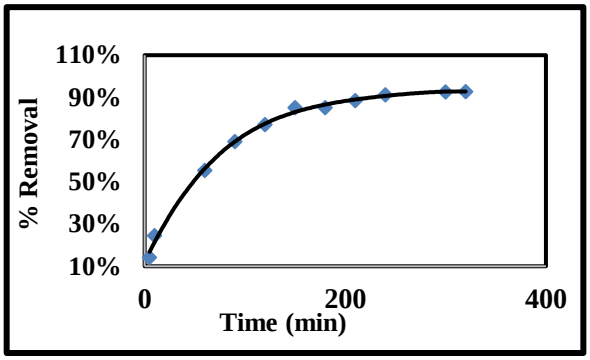

Figure 9: Effect of agitation time on removal % of MG

In the sorption experiment, the effect of contact time is critical since the data would allow confirmation of the agitation time. This will bring the adsorption processes in the solid phase (adsorbent) and the aqueous phase (adsorbates) into equilibrium. The data on the impact of contact time on MG removal is summarized in **Fig. 9.** Generally, on increasing the contact time, the removal efficiency increases and reaches a constant value at equilibrium state[10]. The fast adsorption rate at the initial stage could be explained by the improved availability in the number of active binding sites on the adsorbent surface [68]**,** Moreover, above equilibrium times, the percent removal or the amount of adsorbed dye is not significantly affected because of the saturation of the active sites of the adsorbents [69]. Accordingly, the removal efficiency of MG was increased up to 150 min of contact time, after which, the differences in the removal efficiency were very small. This result is consistent with that of Rahmani et al. [10] and Abdelrahman. [69].

3.3.5. Effect of ionic strength

Fig. 10 is showing the adsorption profile of MG versus different NaCl concentrations in the range of 0.01- 0.5 M, with optimum conditions of pH 7.0, ZM dose of 0.2g, dye concentration of (800 mg/l) and time of 150 min.

Generally, the adsorption efficiency depends on the electrostatic interactions between the cationic dye molecules and the zeolite binding sites [60]. In the present work, MG solutions were prepared with $CaCl_2$ salts having varied metal cationic strengths and the influence of ionic strength of metal cations on adsorption efficiency was examined **Fig. 10**. The results have been confirmed with those of Mittal et al. [60]**,** who found an inverse relation between the ionic strength of a specific cation, such as Na^+ or Ca^{+2}, and its adsorption efficiency. According to the previous authors, the adsorption mechanism of brilliant green dye onto the zeolite-Y-integrated hydrogel composite, followed the ionic interactions, which was highly dependent on the existence of oppositely charged binding sites of zeolite and the brilliant green dye.

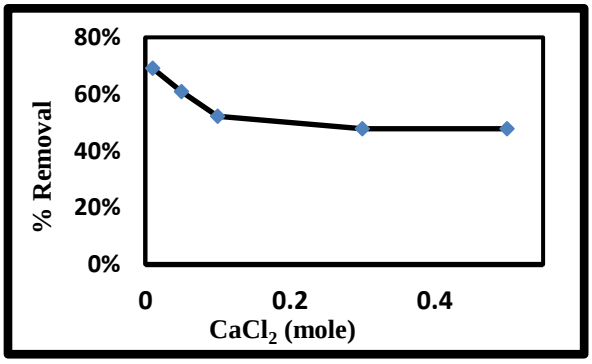

Figure 10: Effect of ions strength on removal% of MG over zeolite

3.3.6. Effect of temperature on the adsorption and thermodynamics

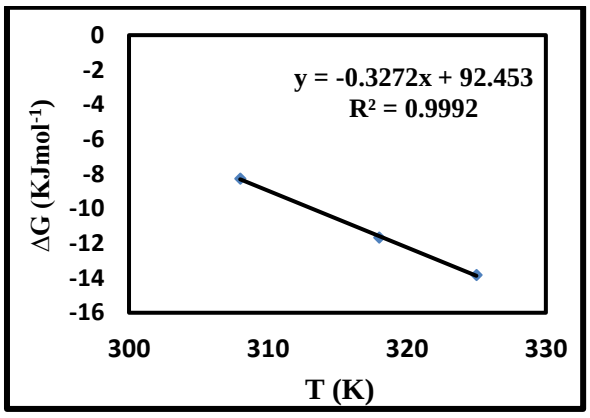

Figure 11: Plots ΔG◦ versus T for adsorption of MG on zeolite

It is well established that, temperature is an additional factor that greatly influence any adsorption process. In the present work, the adsorption of MG was carried out at different temperatures for the initial concentration of 800 mg/l. The free energy of adsorption (ΔG°) was calculated from the following equation:

(B) $\Delta G = - RT \ln K$ **(3)**

where K is the equilibrium constant and T is the solution temperature (K); R is gas constant (8.314 J= mol K). The apparent enthalpy of adsorption (ΔH°) and entropy of adsorption (ΔS°) were calculated from adsorption data at different temperatures using the

Van't Hoff Eq. (4).

$$\ln K = \frac{\Delta S}{R} - \frac{\Delta H}{R}\left(\frac{1}{T}\right) \quad \textbf{(4)}$$

Therefore, batch adsorption experiments were carried out at different temperatures ranging from 308 to 325 K for the zeolite product. Data obtained from the experiments are presented in **Fig. 11**. Values of ΔH ° and ΔS◦ were determined from the slope and intercept of the plot of ΔG◦ versus T. The obtained results from **Table 5** showed that, the obtained ΔG◦ values were found in the range of (-13.82) to (-8.27) kJ/mol, which designated the spontaneous nature of the MG adsorption process. The positive ΔH value supported the improved adsorption efficiencies with increased temperatures and the positive value of ΔS° has suggested the increased randomness at the solid–solution interface during the MG adsorption in aqueous solution on zeolite. These obtained values of ΔG◦, ΔH◦ and ΔS◦ have been found to be in agreement with those reported by Mittal et al. [60], who assigned the adsorption of brilliant green over zeolite-Y to be spontaneous and endothermic in nature. The change in free energy for physisorption and chemisorption was recorded between -20 and 0 kJ/mol, and 80 to-400 kJ/mol, respectively [70]. In Table 5, the obtained value range of ΔG◦ specified the physisorption as the dominating mechanism of MG uptake onto the prepared zeolite surfaces.

Table 5: Thermodynamic parameters for MG adsorption on zeolite under different temperatures.

T	K_a	ΔG	(ΔS) KJ mol^{-1} K^{-1}	(ΔH) KJ mol^{-1}
308	25.29	-8.27	0.33	92.45
318	82.64	-11.67		
325	166.27	-13.82		

3.3.7. Effect of adsorption isotherm

The linear forms of Langmuir, Freundlich, and D-R isotherm equations are given in equations. (5), (6), and (7) respectively, the related constants were calculated and given in Table 3.

$$\frac{Ce}{qe} = \frac{Ce}{q\,max} + \frac{1}{Kqmax} \quad \textbf{(5)}$$

$$\log q = \log Kf + n.\log Ce \quad \textbf{(6)}$$

$$\ln q = \ln qm - K\,\acute{\varepsilon}2\,P \quad \textbf{(7)}$$

where, q_m is the maximum adsorption at monolayer coverage in mg/l; K is the adsorption equilibrium constant related to the energy of adsorption in l/mg; KF and n, Freundlich constants representing the adsorption capacity and intensity respectively; K is the equilibrium constant related to the adsorption energy; ɛp is the Polanyi potential and it was calculated using the following equation:

$$\acute{\varepsilon}p = RT\ln\left(1 + \frac{1}{Ce}\right) \quad \textbf{(8)}$$

where, R is the gas constant (8.13 J) and T is temperature in kelvin. E is the mean free energy of adsorption and can be calculated using the following equation:

$$E = (-2K)^{-0.5} \quad \textbf{(9)}$$

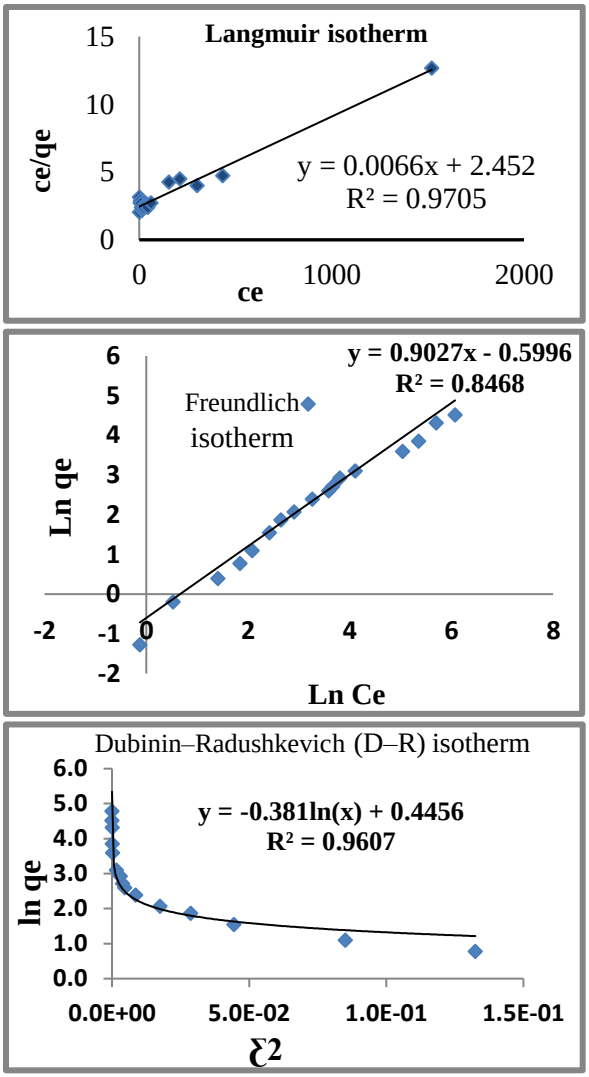

Figure 12: (a): Langumuir adsorption isotherm of MG on zeolite (b); freundlich adsorption isotherm of MG on zeolite (c): Dubinin–Radushkevich (D–R) isotherm of MG on zeolite

As seen in Fig.14, the MG adsorption onto zeolite powder gave a better fit with Langumuir model compared to that of Freundlich and Dubinin–Radushkevich (D–R) isotherm, based on correlation coefficients values (R^2).

The calculated adsorption capacity (V_m= 100 mg/g) that extracted from Langumuir model is obtained close to the experimental value (q_{max}=91.66 mg/g). It can be worthy concluded that, the Langumuir isotherm could be suggested for the monolayer coverage of MG on the surface of the synthetic zeolite. This model proposed that, the surface of zeolite is homogenous and there is a uniform distribution of sites and their energies onto the surface should be without transmigration of adsorbate in the plane of the surface [71]. The same finding was mentioned by Mittal et al. [60] & Abdelrahman, [69], who reported the suitable fitting of langmuir model to the isothermal data of a monolayer homogeneous adsorption of brilliant green over modified zeolite-Y surface, and of MG over a synthesized zeolite nanostructure, respectively.

In order to understand the adsorption type, equilibrium data has been tested by D-R isotherm. Straight lines are obtained by plotting (ln qe) versus (ε2 P), indicating that the adsorption of MG on zeolite obeys the D-R isothermal equation in the entire concentration range. The qm and K` values calculated from the intercepts and slopes of the plots are given in **Fig. 12c.** Based on K values, it is possible to calculate the mean free energy of adsorption (E), which is defined as the free energy change when 1.0 mole of ion is transferred to the surface of the solid from infinity in solution. E value is useful for estimating the type of adsorption and if this value is between 8.0 and 16 Kj/mol, the adsorption type can be explained by ion exchange. The value of E in this study is found within the energy range of physical adsorption (E<8.0) [72]. The calculated value of E is 0.16 K j/mol which is smaller than 8 K j/mol for MG, indicating that adsorption of MG on zeolite is physically in nature.

Table 6: Adsorption isotherm parameters of MG onto zeolite

(A) Langmuir isotherm		
qm(mg/g)	K(l/mg)	R2
100.0	0.000407	0.9705
(B) Freundlich isotherm		
KF	N	R2
0.55	1.19	0.8468
(C) D-R isotherm		
Qm(mg/g)	E (kJ/mol)	R2
14.68	0.61	0.960

3.3.8 Adsorption kinetic

For realizing more data about the adsorption mechanism, different kinetic models are applied; pseudo-first- or pseudo-second-order reaction (Seen Eq. (10) and Eq. (11))

Pseudo first order:

$$\log (qe - qt) = \log qe - \frac{k1}{2.303} t \quad (10)$$

Pseudo − second – order:

$$\frac{t}{qt} = \frac{1}{k2qe2} + \frac{1}{qe} t \quad (11)$$

Where t is the adsorption time, qe and q, (mg/g) are the adsorbed amount of MG at equilibrium and time t and k1, and k2 are the rate constants of pseudo-first order and pseudo-second order, respectively. Adsorption kinetics of MG describes the solute uptake rate and evidently this rate controls the residence time of the adsorbate uptake at the solid–solution interface. Adsorption rate constants for the MG was calculated by using pseudo-first-order and pseudo-second-order kinetic models which were used to describe the mechanism of the adsorption. The conformity between the experimental data and the model-predicted values was expressed by the correlation coefficients (R^2). A relatively high R^2 values indicate that the model has successfully described the kinetics of MG adsorption. **Fig.13** presents the pseudo second-order graphics for the adsorption kinetics of studied dye. The data confirmed good compliance with the second-order kinetic model in terms of higher correlation coefficients (0.9965). In **Table 7,** the regression coefficient (R^2) for second-order model is noticed higher than first-order one. In the other hand, the calculated equilibrium adsorption capacity (qe calc.), extracted from second order is found to be 208.33 mg/g, indicated close agreement with the determined experimental values (qe exp.) 177.15 mg/g. This previous outcome agrees well with the reported data for the adsorption of MG over synthetic and natural zeolites, respectively (Abdelrahman. [69] & Han et al. [9]).

Table 7: Kinetics parameters of MG adsorption by zeolite

adsorbent	parameters	Pseudo first model	Pseudo second model
Zeolite product	R^2	0.8849	0.9652
	$q_{e\ calc.}$	281838.29	208.33333
	$q_{e\ exp.}$	177.15	

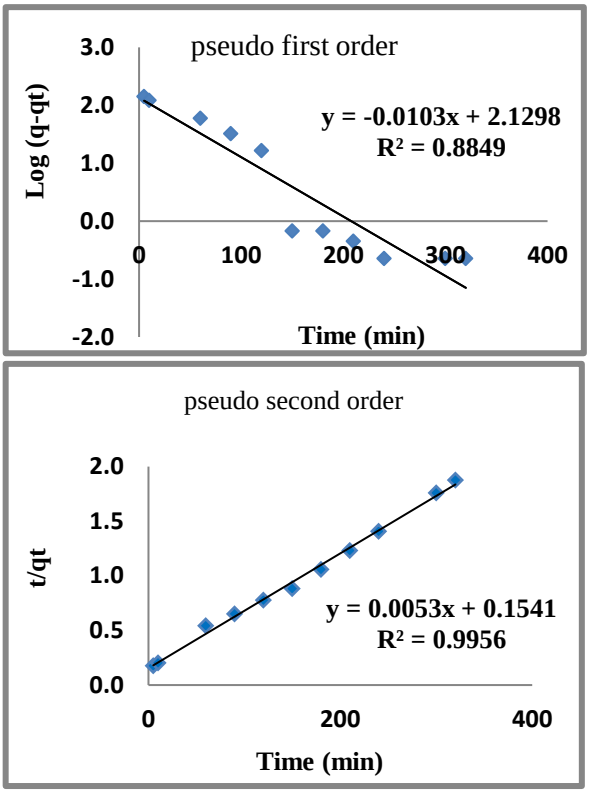

Figure 13: Kinetic plots of pseudo second order for the adsorption of MB over zeolite product.

4. Conclusion

This following data can precisely conclude the major outlies of the in-hand study:

1. A volcanic rock of alkali-andesitic composition was subjected to a zeolitization process at mild hydrothermal lab conditions (1.0M NaOH, 140 ^{o}C, 3day), resulted in an economic microporous adsorbent- mixture containing zeolite-W, Epistilbite, zeolite-X, and Analcime zeolite phases.
2. The synthetic product was efficiently applied with 91.66% MG dye removal capacity, at lab optimum conditions of pH 7.0, ZM dose of 0.2g, dye concentration of 800 mg/l, and optimum time of 150 min.
3. The synthetic product reflected the low-silica and the high alkaline nature of the parent rock, without any negative effect on its adsorption capacity for eliminating MG dye from the effluent solution.
4. The dye molecules were attached on the adsorbent surface via electrostatic interaction mechanism which was confirmed by the reduced adsorption efficiency in presence of other cations like Ca^{+2}. Langmuir model was applied most suitable rather than the other studied isotherm model with correlation coefficient 0.97 to the isotherm data which indicated the monolayer homogeneous adsorption which further increased with increasing temperature. Furthermore, Dubinin Radushkevich has indicated that the adsorption of MG is a physical process. Thermodynamics studies predicted endothermic and spontaneous nature of adsorption. The adsorption kinetics followed pseudo-second order kinetics equation. Therefore, it can be concluded that new synthetic composite of zeolite species is a favorable adsorbent to adsorb cationic dyes with extraordinary adsorption capacity.

5. References

1. Obaid, S. S.; Gaikwad, D.; Sayyed, M.; Khader, A.-R.; Pawar, P., Heavy metal ions removal from waste water bythe natural zeolites. *Materials Today: Proceedings* **2018,** *5* (9), 17930-17934.
2. Shayesteh, H.; Rahbar-Kelishami, A.; Norouzbeigi, R., Adsorption of malachite green and crystal violet cationic dyes from aqueous solution using pumice stone as a low-cost adsorbent: kinetic, equilibrium, and thermodynamic studies. *Desalination and Water Treatment* **2016,** *57* (27), 12822-12831.
3. Zhou, Y.; Lu, J.; Zhou, Y.; Liu, Y., Recent advances for dyes removal using novel adsorbents: a review. *Environmental pollution* **2019,** *252*, 352-365.
4. Kaith, B.; Jindal, R.; Sharma, R., Synthesis of a Gum rosin alcohol-poly (acrylamide) based adsorbent and its application in removal of malachite green dye from waste water. *RSC Advances* **2015,** *5* (54), 43092-43104.
5. Chen, Y.; Zhang, Y.; Liu, C.; Lu, A.; Zhang, W., Photodegradation of malachite green by nanostructured Bi 2 WO 6 visible light-induced photocatalyst. *International Journal of Photoenergy* **2011,** *2012*.
6. Qadeer, R., Adsorption behavior of ruthenium ions on activated charcoal from nirtic acid medium. *Colloids and Surfaces A: Physicochemical and Engineering Aspects* **2007,** *293* (1-3), 217-223.
7. Jha, B.; Singh, D., A review on synthesis, characterization and industrial applications of flyash zeolites. *Journal of Materials Education* **2011,** *33* (1), 65.
8. Rafatullah, M.; Sulaiman, O.; Hashim, R.; Ahmad, A., Adsorption of methylene blue on low-cost adsorbents: a review. *Journal of hazardous materials* **2010,** *177* (1-3), 70-80.
9. Han, R.; Wang, Y.; Sun, Q.; Wang, L.; Song, J.; He, X.; Dou, C., Malachite green adsorption onto natural zeolite and reuse by microwave

irradiation. *Journal of Hazardous Materials* **2010,** *175* (1-3), 1056-1061.
10. Rahmani, M.; Kaykhaii, M.; Sasani, M., Application of Taguchi L16 design method for comparative study of ability of 3A zeolite in removal of Rhodamine B and Malachite green from environmental water samples. *Spectrochimica Acta Part A: Molecular and Biomolecular Spectroscopy* **2018,** *188*, 164-169.
11. Pereira, P. M.; Ferreira, B. F.; Oliveira, N. P.; Nassar, E. J.; Ciuffi, K. J.; Vicente, M. A.; Trujillano, R.; Rives, V.; Gil, A.; Korili, S., Synthesis of zeolite A from metakaolin and its application in the adsorption of cationic dyes. *Applied Sciences* **2018,** *8* (4), 608.
12. (a) Collins, F.; Rozhkovskaya, A.; Outram, J. G.; Millar, G. J., A critical review of waste resources, synthesis, and applications for Zeolite LTA. *Microporous and mesoporous Materials* **2020,** *291*, 109667; (b) Maia, A. Á. B.; Dias, R. N.; Angélica, R. S.; Neves, R. F., Influence of an aging step on the synthesis of zeolite NaA from Brazilian Amazon kaolin waste. *Journal of Materials Research and Technology* **2019,** *8* (3), 2924-2929; (c) Garcia, G.; Cabrera, S.; Hedlund, J.; Mouzon, J., Selective synthesis of FAU-type zeolites. *Journal of Crystal Growth* **2018,** *489*, 36-41.
13. Luo, H.; Law, W. W.; Wu, Y.; Zhu, W.; Yang, E.-H., Hydrothermal synthesis of needle-like nanocrystalline zeolites from metakaolin and their applications for efficient removal of organic pollutants and heavy metals. *Microporous and Mesoporous Materials* **2018,** *272*, 8-15.
14. Tong, C.; Hou, J.; Yang, C., Preparation of NH4+-loaded merlinoite for extracting potassium continuously at room temperature. *Journal of Industrial and Engineering Chemistry* **2019,** *80*, 11-16.
15. Kakutani, Y.; Weerachawanasak, P.; Hirata, Y.; Sano, M.; Suzuki, T.; Miyake, T., Highly effective K-Merlinoite adsorbent for removal of Cs+ and Sr 2+ in aqueous solution. *RSC advances* **2017,** *7* (49), 30919-30928.
16. Li, J.; Zhuang, X.; Font, O.; Moreno, N.; Vallejo, V. R.; Querol, X.; Tobias, A., Synthesis of merlinoite from Chinese coal fly ashes and its potential utilization as slow release K-fertilizer. *Journal of hazardous materials* **2014,** *265*, 242-252.
17. Jin, N.; Meng, C.; Hou, J., Preparation and characterization of merlinoite for potassium extraction from seawater. *Journal of Industrial and Engineering Chemistry* **2014,** *20* (4), 1227-1230.
18. Seo, Y.-H.; Prasetyanto, E. A.; Jiang, N.; Oh, S.-M.; Park, S.-E., Catalytic dehydration of methanol over synthetic zeolite W. *Microporous and Mesoporous Materials* **2010,** *128* (1-3), 108-114.
19. Maghsoodloorad, H.; Mirfendereski, S. M.; Mohammadi, T.; Pak, A., Effects of gel parameters on the synthesis and characteristics of W-type zeolite nanoparticles. *Clays and Clay Minerals* **2011,** *59* (3), 328-335.
20. Thoma, S. G.; Nenoff, T. M., A novel synthesis of zeolite W using organometallic precursors. *Microporous and mesoporous materials* **2000,** *34* (3), 301-306.
21. Cichocki, A.; Kościelniak, P., Experimental designs applied to hydrothermal synthesis of zeolite ERI+ OFF (T) in the Na2O–K2O–Al2O3–SiO2–H2O system: part 2. Regular study. *Microporous and mesoporous materials* **1999,** *29* (3), 369-382.
22. Youssef, H. F., Ismail, N, Microwave- Assisted Synthesis of Nano/Micronized Zeolites from Natural Sources: Evaluation of Hydrogen Storage Capacities. *Egypt. J. Chem* **2020,** *10* (63), 3669 – 3683.
23. Abdelrahman, E. A.; Alharbi, A.; Subaihi, A.; Hameed, A. M.; Almutairi, M. A.; Algethami, F. K.; Youssef, H. M., Facile fabrication of novel analcime/sodium aluminum silicate hydrate and zeolite Y/faujasite mesoporous nanocomposites for efficient removal of Cu (II) and Pb (II) ions from aqueous media. *Journal of Materials Research and Technology* **2020,** *9* (4), 7900-7914.
24. Yang, D.; Chu, Z.; Zheng, R.; Wei, W.; Feng, X.; Zhang, J.; Li, C.; Zhang, Z.; Chen, H., Remediation of Cu-polluted soil with analcime synthesized from engineering abandoned soils through green chemistry approaches. *Journal of Hazardous Materials* **2021,** *406*, 124673.
25. Azizi, S. N.; Ghasemi, S.; Derakhshani-mansoorkuhi, M., The synthesis of analcime zeolite nanoparticles using silica extracted from stem of sorghum Halepenesic ash and their application as support for electrooxidation of formaldehyde. *International Journal of Hydrogen Energy* **2016,** *41* (46), 21181-21192.
26. (a) SAKIZCI, M., Investigation of thermal and structural properties of natural and ion-exchanged analcime. *Anadolu University Journal of Science and Technology A-Applied Sciences and Engineering* **2016,** *17* (4), 724-734; (b) Colella, C.; Wise, W. S., The IZA Handbook of Natural Zeolites: A tool of knowledge on the most important family of porous minerals. *Microporous and Mesoporous Materials* **2014,** *189*, 4-10.
27. Atta, A.; Jibril, B.; Aderemi, B.; Adefila, S., Preparation of analcime from local kaolin and rice husk ash. *Applied Clay Science* **2012,** *61*, 8-13.

28. Rachkova, N.; Taskaev, A., Immobilization of U, Ra, and Th compounds with analcime-containing rock and hydrolysis lignin. *Radiochemistry* **2011,** *53* (3), 314-321.
29. Hernandez-Espinosa, M. A.; Quiroz-Estrada, K.; Petranovskii, V.; Rojas, F.; Portillo, R.; Salgado, M. A.; Marcelo, M.; Rubio, E.; Felipe, C., Adsorption of N2, NO2 and CO2 on Epistilbite Natural Zeolite from Jalisco, Mexico after Acid Treatment. *Minerals* **2018,** *8* (5), 196.
30. Wang, Y.; Jia, H.; Chen, P.; Fang, X.; Du, T., Synthesis of La and Ce modified X zeolite from rice husk ash for carbon dioxide capture. *Journal of Materials Research and Technology* **2020,** *9* (3), 4368-4378.
31. Nonnen, T.; Preißler, H.; Kött, S.; Beckert, S.; Gläser, R., Salt inclusion and deliquescence in salt/zeolite X composites for thermochemical heat storage. *Microporous and Mesoporous Materials* **2020,** *303*, 110239.
32. Zhang, S.; Cui, M.; Chen, J.; Ding, Z.; Wang, X.; Mu, Y.; Meng, C., Modification of synthetic zeolite X by thiourea and its adsorption for Cd (II). *Materials Letters* **2019,** *236*, 233-235.
33. Yang, T.; Han, C.; Liu, H.; Yang, L.; Liu, D.; Tang, J.; Luo, Y., Synthesis of Na-X zeolite from low aluminum coal fly ash: characterization and high efficient As (V) removal. *Advanced Powder Technology* **2019,** *30* (1), 199-206.
34. Yan, J.; Li, Y.; Li, H.; Zhou, Y.; Xiao, H.; Li, B.; Ma, X., Effective removal of ruthenium (III) ions from wastewater by amidoxime modified zeolite X. *Microchemical Journal* **2019,** *145*, 287-294.
35. Geologyscience.com Andesite. https://geologyscience.com/rocks/igneous-rocks/andesite

(accessed).
36. Sogancioglu, M.; Yel, E.; Yilmaz-Keskin, U. S., Utilization of andesite processing wastewater treatment sludge as admixture in concrete mix. *Construction and Building Materials* **2013,** *46*, 150-155.
37. Guang-hua, F., China's Maifanshi resources and their development and research. *Bulletin of Mineralogy, Petrology and Geochemistry* **2001,** *20*, 131-135.
38. (a) Elfeky, A. S.; Youssef, H. F.; Elzaref, A. S., Adsorption of dye from wastewater onto ZnO nanoparticles-loaded zeolite: kinetic, thermodynamic and isotherm studies. *Zeitschrift für Physikalische Chemie* **2020,** *234* (2), 255-278; (b) Jamil, T. S.; Youssef, H., Microwave synthesis of zeolites from Egyptian kaolin: Evaluation of heavy metals removal. *Separation Science and Technology* **2016,** *51* (18), 2876-2886.
39. Passaglia, E.; Pongiluppi, D.; Rinaldi, R., Merlinoite, a new mineral of the zeolite group. *Neues Jahrbuch für Mineralogie, Monatshefte* **1977,** *1977*, 355-364.
40. Baerlocher, C.; McCusker, L. B.; Olson, D. H., *Atlas of zeolite framework types*. Elsevier: 2007.
41. (a) Donahoe, R. J.; Hemingway, B. S.; Liou, J., Thermochemical data for merlinoite; 1, Low-temperature heat capacities, entropies, and enthalpies of formation at 298.15 K of six synthetic samples having various Si/Al and Na/(Na+ K) ratios. *American Mineralogist* **1990,** *75* (1-2), 188-200; (b) Colella, C., Aiello, R . , a n d D i L u d o v i c o , V, Synthesis of merlinoite. *Soc. Ital. Mineral. Petrol* **1977,** *33*, 511-518; (c) Barrer, R. M.; Baynham, J., 562. The hydrothermal chemistry of the silicates. Part VII. Synthetic potassium aluminosilicates. *Journal of the Chemical Society (Resumed)* **1956**, 2882-2891.
42. (a) Yeo, Z. Y.; Chai, S.-P.; Zhu, P. W.; Mah, S.-K.; Mohamed, A. R., Preparation of self-supported crystalline merlinoite-type zeolite W membranes through vacuum filtration and crystallization for CO 2/CH 4 separations. *New Journal of Chemistry* **2015,** *39* (5), 4135-4140; (b) Worathanakul, P.; Trisuwan, D.; Phatruk, A.; Kongkachuichay, P., Effect of sol–gel synthesis parameters and Cu loading on the physicochemical properties of a new SUZ-4 zeolite. *Colloids and Surfaces A: Physicochemical and Engineering Aspects* **2011,** *377* (1-3), 187-194.
43. IZA, Database of Zeolite Structures

Available online: http://www.iza-structure.org/databases

2017.
44. Index of Natural Zeolites Datasheets

Available online: http://www.iza-online.org/natural/IZA-NZ_Datasheets.htm
2017.
45. Tümsek, F.; İnel, O., Evaluation of the thermodynamic parameters for the adsorption of some n-alkanes on A type zeolite crystals by inverse gas chromatography. *Chemical Engineering Journal* **2003,** *94* (1), 57-66.
46. Khabashesku, V., Mazyar, O., Chakraborty, S., Agrawal, G., & Hain, T. D., *U.S. Patent No. 9,012,377. Washington, DC: U.S. Patent and Trademark Office.*٢٠١٥ .
47. Field, B. F., Apparatus for Cleaning a Surface Comprises A Mobile Body; First Liquid Line Configured to Receive a Liquid; a Container Coupled to the First Liquid Line; a Second Liquid Line Coupled to the Container; and Dispenser. *Patent No. US2010276301-A1*.

2010.

48. Meier, W. M.; Olson, D. H.; Baerlocher, C., Atlas of the zeolite structure types. *Zeolites* **1996,** *17* (1-2).
49. Saha, P., Geochemical and X-ray investigation of natural and synthetic analcites. *American Mineralogist: Journal of Earth and Planetary Materials* **1959,** *44* (3-4), 300-313.
50. Palubinskaite, D.; Sinkeviciene, I.; Siauciunas, R.; Sadunas, A., Determination of the parameters of Analcime synthesis and the obtaining of Leucite by ion exchange. *Sci* **2000,** *6* (1), 36-43.
51. Bejar, A.; Chaabene, S. B.; Jaber, M.; Lambert, J.-F.; Bergaoui, L., Mn-analcime: synthesis, characterization and application to cyclohexene oxidation. *Microporous and mesoporous materials* **2014,** *196*, 158-164.
52. Dyer, A.; Tangkawanit, S.; Rangsriwatananon, K., Exchange diffusion of Cu2+, Ni2+, Pb2+ and Zn2+ into analcime synthesized from perlite. *Microporous and mesoporous materials* **2004,** *75* (3), 273-279.
53. Liu, B.; Tang, D.; Au, C., Fabrication of analcime zeolite fibers by hydrothermal synthesis. *Microporous and Mesoporous Materials* **2005,** *86* (1-3), 106-111.
54. Balandis, A.; Traidaraite, A., The influence of Al containing component on synthesis of analcime of various crystallographic systems. *Materials Science-Poland* **2007,** *25* (3), 637-647.
55. Jacobs, P.; Flanigen, E. M.; Jansen, J.; van Bekkum, H., *Introduction to zeolite science and practice*. Elsevier: 2001.
56. (a) Patdhanagul, N.; Srithanratana, T.; Rangsriwatananon, K.; Hengrasmee, S., Ethylene adsorption on cationic surfactant modified zeolite NaY. *Microporous and Mesoporous Materials* **2010,** *131* (1-3), 97-102; (b) Chaouati, N.; Soualah, A.; Chater, M., Adsorption of phenol from aqueous solution onto zeolites Y modified by silylation. *Comptes Rendus Chimie* **2013,** *16* (3), 222-228.
57. (a) Neidrauer, M.; Ercan, U. K.; Bhattacharyya, A.; Samuels, J.; Sedlak, J.; Trikha, R.; Barbee, K. A.; Weingarten, M. S.; Joshi, S. G., Antimicrobial efficacy and wound-healing property of a topical ointment containing nitric-oxide-loaded zeolites. *Journal of medical microbiology* **2014,** *63* (Pt 2), 203; (b) Vilaça, N.; Amorim, R.; Machado, A. F.; Parpot, P.; Pereira, M. F.; Sardo, M.; Rocha, J.; Fonseca, A. M.; Neves, I. C.; Baltazar, F., Potentiation of 5-fluorouracil encapsulated in zeolites as drug delivery systems for in vitro models of colorectal carcinoma. *Colloids and Surfaces B: Biointerfaces* **2013,** *112*, 237-244.
58. Babajide, O.; Musyoka, N.; Petrik, L.; Ameer, F., Novel zeolite Na-X synthesized from fly ash as a heterogeneous catalyst in biodiesel production. *Catalysis Today* **2012,** *190* (1), 54-60.
59. El-Naggar, M.; El-Kamash, A.; El-Dessouky, M.; Ghonaim, A., Two-step method for preparation of NaA-X zeolite blend from fly ash for removal of cesium ions. *Journal of Hazardous Materials* **2008,** *154* (1-3), 963-972.
60. Mittal, H.; Babu, R.; Dabbawala, A. A.; Stephen, S.; Alhassan, S. M., Zeolite-Y incorporated karaya gum hydrogel composites for highly effective removal of cationic dyes. *Colloids and Surfaces A: Physicochemical and Engineering Aspects* **2020,** *586*, 124161.
61. Della Ventura, G.; Parodi, G.; Burragato, F.; Mottana, A., Nuovi dati sulla merlinoite e su zeoliti affini. *Rendiconti Lincei* **1993,** *4*, 303-313.
62. (a) Christidis, G.; Paspaliaris, I.; Kontopoulos, A., Zeolitisation of perlite fines: mineralogical characteristics of the end products and mobilization of chemical elements. *Applied Clay Science* **1999,** *15* (3-4), 305-324; (b) Troger , W. E., Optische Bestimmung der gesteinsbildenden Minerale, . *Teil 2, Schweizerbart'sche Verlagsbuchhandlung, Stuttgart*, **1967**, 788.
63. (a) Osacký, M.; Pálková, H.; Hudec, P.; Czímerová, A.; Galusková, D.; Vítková, M., Effect of alkaline synthesis conditions on mineralogy, chemistry and surface properties of phillipsite, P and X zeolitic materials prepared from fine powdered perlite by-product. *Microporous and Mesoporous Materials* **2020,** *294*, 109852; (b) Zaarour, M.; Dong, B.; Naydenova, I.; Retoux, R.; Mintova, S., Progress in zeolite synthesis promotes advanced applications. *Microporous and Mesoporous Materials* **2014,** *189*, 11-21; (c) Mintova, S.; Olson, N. H.; Valtchev, V.; Bein, T., Mechanism of zeolite A nanocrystal growth from colloids at room temperature. *Science* **1999,** *283* (5404), 958-960; (d) Hay, R. L.; Sheppard, R. A., Occurrence of zeolites in sedimentary rocks: An overview. *Reviews in mineralogy and geochemistry* **2001,** *45* (1), 217-234.
64. Oelkers, E. H.; Schott, J., Experimental study of anorthite dissolution and the relative mechanism of feldspar hydrolysis. *Geochimica et Cosmochimica Acta* **1995,** *59* (24), 5039-5053.
65. Paul, D.; Kasera, N.; Kolar, P.; Hall, S. G., Physicochemical characterization data of pine-derived biochar and natural zeolite as precursors to catalysts. *Chemical Data Collections* **2020,** *30*, 100573.

66. Garg, V.; Gupta, R.; Yadav, A. B.; Kumar, R., Dye removal from aqueous solution by adsorption on treated sawdust. *Bioresource technology* **2003,** *89* (2), 121-124.
67. Kragović, M.; Stojmenović, M.; Petrović, J.; Loredo, J.; Pašalić, S.; Nedeljković, A.; Ristović, I., Influence of alginate encapsulation on point of zero charge (pHpzc) and thermodynamic properties of the natural and Fe (III)-modified zeolite. *Procedia Manufacturing* **2019,** *32*, 286-293.
68. Saha, P.; Chowdhury, S.; Gupta, S.; Kumar, I., Insight into adsorption equilibrium, kinetics and thermodynamics of Malachite Green onto clayey soil of Indian origin. *Chemical Engineering Journal* **2010,** *165* (3), 874-882.
69. Abdelrahman, E. A., Synthesis of zeolite nanostructures from waste aluminum cans for efficient removal of malachite green dye from aqueous media. *Journal of Molecular Liquids* **2018,** *253*, 72-82.
70. Tehrani-Bagha, A.; Nikkar, H.; Mahmoodi, N.; Markazi, M.; Menger, F., The sorption of cationic dyes onto kaolin: Kinetic, isotherm and thermodynamic studies. *Desalination* **2011,** *266* (1-3), 274-280.
71. Sartape, A. S.; Mandhare, A. M.; Jadhav, V. V.; Raut, P. D.; Anuse, M. A.; Kolekar, S. S., Removal of malachite green dye from aqueous solution with adsorption technique using Limonia acidissima (wood apple) shell as low cost adsorbent. *Arabian Journal of Chemistry* **2017,** *10*, S3229-S3238.
72. Çalışkan, E.; Göktürk, S., Adsorption characteristics of sulfamethoxazole and metronidazole on activated carbon. *Separation Science and Technology* **2010,** *45* (2), 244-255.